AIAA Guidance, Navigation, and Control Conference and Exhibit
21 - 24 August 2006, Keystone, Colorado

AIAA 2006-6351

Development of UAV Navigation System Based on Unscented Kalman Filter

Seung-Min Oh* and Eric N. Johnson †

School of Aerospace Engineering, Georgia Institute of Technology, Atlanta, GA 30332

This paper describes the detailed development and implementation of a low-cost strapdown inertial navigation system and its application to the navigation of an Unmanned Aerial Vehicle (UAV). The navigation system fuses various sources of information from low-cost sensor suites such as an Inertial Measurement Unit (IMU), a Global Positioning System (GPS), and a three-axis magnetometer in the framework of an Unscented Kalman Filter (UKF). In particular, sensor measurements are taken at various rates and states are updated based on the availability of these measurements. The performance and error analysis of the overall integrated navigation system are assessed in a realistic simulation environment by comparing performance with that of an existing Extended Kalman Filter-based navigation system.

Nomenclature

$\mathbf{r}^n$	position vector of the vehicle in navigation frame
$\mathbf{v}^n$	velocity vector of the vehicle in navigation frame
$\mathbf{q}$	quaternion vector which describes vehicle attitude
$\mathbf{b}_a$	IMU accelerometer bias vector
$\mathbf{b}_\omega$	IMU rate gyro bias vector
$\mathbf{a}_{cg}^b$	specific force vector of the vehicle in body frame
$\mathbf{x}$	state vector of process model
$\mathbf{C}_b^n$	direction cosine matrix (DCM) or transformation matrix from body frame to navigation frame
$\mathbf{r}_{gps}^b$	GPS antenna position vector relative to vehicle C.G. location in body frame, $\mathbf{r}_{gps}^b = [\ x_g\ y_g\ z_g\ ]^T$
$\mathbf{r}_{imu}^b$	IMU position vector relative to vehicle center of gravity in body frame, $\mathbf{r}_{imu}^b = [\ x_a\ y_a\ z_a\ ]^T$
$\mathbf{g}^n$	gravity vector in navigation frame
$\mathbf{n}_a$	ãccelerometer triads noise vector
$\boldsymbol{n}_\omega$	rate gyro triads noise vector

Subscript or Superscript

k	time index
m	measurement
ω	rate gyro or angular rate
b	body frame
n	navigation frame

I. Introduction

RECENTLY, due to the easy availability of low-cost inertial measurement unit (IMU) consisting of accelerometer and rate gyro triads, rigidly mounted on a vehicle, inertial navigation system (INS) has become a backbone in cost-effective autonomous unmanned aerial vehicles (UAVs). INS can provide high rate vehicle position, velocity, and attitude information necessary for flight GNC (Guidance, navigatgion,

*Graduate Research Assistant, Student Member AIAA, gtg895i@mail.gatech.edu.
†Lockheed Martin Assistant Professor of Avionics Integration, Member AIAA, Eric.Johnson@ae.gatech.edu

and control) system. The measured three axis accelerations and angular rates from accelerometer and rate gyro triads, respectively, are integrated to obtain the vehicle's position, velocity, and attitude in an on-board computer. Since vehicle's acceleration from accelerometer and angular rate from rate gyro are generally susceptible to various measurement noise sources, the accuracy of position/velocity and attitude information degrades with time.[1,2,3,4,5] Increasing the navigation accuracy by incorporating more accurate IMU measurement devices makes the INS system very expensive. On the other hand, recent research shows that the growth of numerical errors in IMU navigation with time can be prevented by using low-cost absolute aiding sensors such as Global Positioning System (GPS), magnetometer, altimeter, and so on.[6,7,8,9,10,11] By combining the low-cost IMU with absolute aiding sensors, relatively accurate state estimation information can be provided to low-cost autonomous small UAV navigation system. This integrated navigation system solves the time-degrading accuracy problem of INS by combining short term high rate data characteristics of INS with low rate but relatively time-independent accuracy of absolute aiding sensors. Since accelerometer and rate gyro data (from an IMU) and aiding sensor measurements usually include various sources of noise, navigation estimate accuracy is highly dependent on noise filtering details.

Figure 1. GTMax Research UAV

Typically, long term INS errors are corrected by fusing IMU measurements with aiding sensor measurements such as GPS position/velocity, magnetometer heading information, and so on in the framework of extended Kalman filter (EKF).[5,12,7,8,9] Recently, unscented Kalman filter (UKF) draws much research attention mainly because of its several salient features.[13,14,15] UKF can be applied directly to nonlinear system. Hence it is not necessary to compute Jacobian matrix which should be provided in order to use an EKF. The EKF is based on first order gradient information of nonlinear system and thus its accuracy is known to be first order, while UKF incorporates higher order gradient information and therefore it is known as more accurate.

The purpose of this research is to develop UKF-based integrated navigation system based on the existing EKF-based system well described in Ref. 6,16,17. The developed algorithmic details are targeting to implement on low-cost strapdown inertial navigation systems with application to Research Unmanned Aerial Vehicle (UAV)[18,19,6,16] shown in figure 1.

The paper is organized as follows. Section II discusses the overall INS algorithm with the derivation of detailed process model which will be used in EKF/UKF-based navigation filter. The measurement models with specific sensor hardware characteristics are presented in section III. The overall EKF algorithm with sequential measurement update and UKF formualtion are summarized in section IV. Some simulation results with both EKF and UKF navigation filters present the comparison of two filter performance in section V. Finally, section VI summarizes the paper.

II. Inertial Navigation System Description

The combination of IMU hardware, composed of accelerometer triad and rate gyro triad, and navigation software that includes appropriate navigation algorithms is called an inertial navigation system (INS). INS can determine position, velocity, and attitude of a vehicle by measuring three-axis accelerations from accelerometer triad and three-axis angular rates from rate gyro triad. The fundamental part of navigation algorithms is navigation equation. The navigation equation for UAV local navigation can be expressed as follows:[3]

$$\frac{d^2\mathbf{r}^n}{dt^2} = \mathbf{a}^n_{cg} + \mathbf{g}^n. \tag{1}$$

This equation provides, with proper integration, the navigation quantities of velocity and position, thus it is called the navigation equation. Since we are developing the INS for autonomous research UAV flying in locally limited area, Earth curvature and Earth rotation effect are neglected (flat Earth and inertially fixed Earth assumption). This is reasonable assumption for our purpose.[7] Velocity of a vehicle can be obtained

by time-integrating once the above navigation equation as in

$$\mathbf{v}^n = \frac{d\mathbf{r}^n}{dt} \tag{2}$$

and its position, $\mathbf{r}^n$, can be obtained by integrating twice. The accelerometer triad and rate gyro triad in the strapdown INS, adopted in our UAV navigation, are rigidly fixed in the vehicle. This means that the accelerometer measurements or specific forces from accelerometer triad are obtained in body frame, hence they need to be transformed to navigation frame in order to be used in navigation equation.

$$\mathbf{a}_{cg}^n = \mathbf{C}_b^n \mathbf{a}_{cg}^b, \tag{3}$$

where $\mathbf{C}_b^n$ is the direction cosine matrix (DCM) from body-fixed frame to the navigation frame. Then the navigation equation becomes:

$$\frac{d^2\mathbf{r}^n}{dt^2} = \mathbf{C}_b^n \mathbf{a}_{cg}^b + \mathbf{g}^n. \tag{4}$$

The transformation matrix, $\mathbf{C}_b^n$, is time-varying quantity and is a function of current attitude. In order to determine current attitude, we need an attitude evolution equation. Depending on which parameter set is used to express attitude, attitude equation varies in different form. Two most popular ways to express attitude are using three parameters of Euler angles ($\phi,\ \theta,\ \psi$) and four parameters of a quaternion ($q_0,\ q_1,\ q_2,\ q_3$). Both ways have advantages and disadvantages. Using Euler angles is more intuitive to express the attitude but involves complex trigonometric relations in attitude equation. On the other hand, the attitude equation is simple and without any trigonometric term when we use a quaternion as attitude parameters. In our research, quaternion set is used as the attitude parameters resulting in the following attitude equation:

$$\dot{\mathbf{q}} = \frac{1}{2}\mathbf{\Omega}(\boldsymbol{\omega}^b)\mathbf{q} = \frac{1}{2}\mathbf{Z}(\mathbf{q})\boldsymbol{\omega}^b, \tag{5}$$

where $\mathbf{\Omega}$ and $\mathbf{Z}$ are given below.

With the vehicle's angular rate vector $\boldsymbol{\omega}^b(t)$ from rate gyro triad and initial quaternion vector $\mathbf{q}(t=0)$, this attitude equation can be integrated to get quaternion vector or attitude at any time, $\mathbf{q}(t)$.
Combining the navigation equation, Eq. (4), expressed in state space form by using the vehicle's velocity vector in Eq. (2) and attitude equation, Eq. (5), we get the following ideal INS mechnization equations:

$$\dot{\mathbf{r}}^n = \mathbf{v}^n, \tag{6}$$

$$\dot{\mathbf{v}}^n = \mathbf{C}_b^n(\mathbf{q})\ \mathbf{a}_{cg}^b + \mathbf{g}^n, \tag{7}$$

$$\dot{\mathbf{q}} = \frac{1}{2}\mathbf{\Omega}(\boldsymbol{\omega}^b)\ \mathbf{q} = \frac{1}{2}\mathbf{Z}(\mathbf{q})\ \boldsymbol{\omega}^b, \tag{8}$$

where

$$\mathbf{C}_b^n = (\mathbf{C}_n^b)^T = \begin{bmatrix} 1-2(q_2^2+q_3^2) & 2(q_1q_2-q_0q_3) & 2(q_1q_3+q_0q_2) \\ 2(q_1q_2+q_0q_3) & 1-2(q_1^2+q_3^2) & 2(q_2q_3-q_0q_1) \\ 2(q_1q_3-q_0q_2) & 2(q_2q_3+q_0q_1) & 1-2(q_1^2+q_2^2) \end{bmatrix}, \tag{9}$$

$$\mathbf{\Omega}(\boldsymbol{\omega}^b) = \begin{bmatrix} 0 & -\boldsymbol{\omega}^{bT} \\ \boldsymbol{\omega}^b & -\tilde{\boldsymbol{\omega}}^b \end{bmatrix} = \begin{bmatrix} 0 & -\omega_1 & -\omega_2 & -\omega_3 \\ \omega_1 & 0 & \omega_3 & -\omega_2 \\ \omega_2 & -\omega_3 & 0 & \omega_1 \\ \omega_3 & \omega_2 & -\omega_1 & 0 \end{bmatrix},\ \boldsymbol{\omega}^b = \begin{bmatrix} \omega_1 \\ \omega_2 \\ \omega_3 \end{bmatrix},\ \tilde{\boldsymbol{\omega}}^b = \begin{bmatrix} 0 & -\omega_3 & \omega_2 \\ \omega_3 & 0 & -\omega_1 \\ -\omega_2 & \omega_1 & 0 \end{bmatrix}, \tag{10}$$

$$\mathbf{Z}(\mathbf{q}) = \begin{bmatrix} -\mathbf{q}_{13}^T \\ \tilde{\mathbf{q}}_{13} + q_0\ \mathbf{I}_{3\times 3} \end{bmatrix} = \begin{bmatrix} -q_1 & -q_2 & -q_3 \\ q_0 & -q_3 & q_2 \\ q_3 & q_0 & -q_1 \\ -q_2 & q_1 & q_0 \end{bmatrix},\ \mathbf{q} = \begin{bmatrix} q_0 \\ \mathbf{q}_{13} \end{bmatrix} = \begin{bmatrix} q_0 \\ q_1 \\ q_2 \\ q_3 \end{bmatrix},\ \tilde{\mathbf{q}}_{13} = \begin{bmatrix} 0 & -q_3 & q_2 \\ q_3 & 0 & -q_1 \\ -q_2 & q_1 & 0 \end{bmatrix}, \tag{11}$$

$$q_0^2+q_1^2+q_2^2+q_3^2 = 1,\ \ \mathbf{g}^n = \begin{bmatrix} 0 & 0 & g \end{bmatrix}^T. \tag{12}$$

The magnitude of gravity at the surface of the WGS-84 ellipsoid can be expressed in the form:[2]

$$g = g_0 \frac{1 + g_1 \ sin^2\phi_{lat}}{(1 - \epsilon^2 \ sin^2\phi_{lat})^{\frac{1}{2}}}, \tag{13}$$

where ϕ_{lat} is geodetic latitude, $g_0 = 9.7803267714 \ m/sec^2$ is the gravity at equator, $g_1 = 0.00193185138639$ m/sec^2 is gravity formula constant, and $\epsilon = 0.0818191908426$ is the first eccentricity.

The states of the ideal INS mechanization in Eq. (6) $\sim$ (8) include three components of positions, three components of velocities, and four quaternions. IMU is considered to provide three accelerations from accelerometer triad and three angular rates from rate gyro triad.

A. Continuous Process Model of INS Navigation

Since extended Kalman filter is based on continuous time process model in our research (Ref. 18,19,6,16,17), we first derive continuous time process model for our integrated INS navigation system. The Ideal INS equations in Eq. (6) $\sim$ (8) are derived based on the assumption that IMU is positioned at the vehicle's center of gravity and hence accelerometer triad measures acceleration at the center of gravity. Due to space limitation or installation convenience, IMU is usually positioned at some position, $\mathbf{r}^b_{imu}$, relative to the vehicle's center of gravity. Acceleration vector at IMU position, $\mathbf{a}^b$, can be calculated from the following relation:

$$\mathbf{a}^b = \mathbf{a}^b_{cg} + \Delta\mathbf{a}^b_{imu}, \tag{14}$$

where

$$\Delta\mathbf{a}^b_{imu} = \dot{\boldsymbol{\omega}}^b \times \mathbf{r}^b_{imu} + \boldsymbol{\omega}^b \times \left(\boldsymbol{\omega}^b \times \mathbf{r}^b_{imu}\right), \tag{15}$$

$\Delta\mathbf{a}^b_{imu}$ is the acceleration effect due to the IMU offset from the vehicle's center of gravity location, $\mathbf{r}^b_{imu}$. Since the rate gyro triad are rigidly fixed to the vehicle, angular rates at IMU position are the same as those at vehicle's center of gravity. Hence, we do not differentiate between the two.

In general, the IMU sensor measurements are corrupted by various types of errors such as scale factors, misalignments, biases, and random noises.[2,20,7,21] So the sensor models can be detailed depending on required navigation accuracy and inertial sensors at hand. In the INS development of our autonomous research UAV, it was enough to consider that true values are perturbed by two effects, a bias and a measurement noise in both the acceleration and rate gyro measurements.[16,11,22]

$$\begin{aligned} \mathbf{a}^b_m &= \mathbf{a}^b + \mathbf{b}_a + \mathbf{n}_a, \\ \boldsymbol{\omega}^b_m &= \boldsymbol{\omega}^b + \mathbf{b}_\omega + \mathbf{n}_\omega \end{aligned} \tag{16}$$

or

$$\begin{aligned} \mathbf{a}^b &= \mathbf{a}^b_m - \mathbf{b}_a - \mathbf{n}_a = \bar{\mathbf{a}}^b - \mathbf{n}_a, \\ \boldsymbol{\omega}^b &= \boldsymbol{\omega}^b_m - \mathbf{b}_\omega - \mathbf{n}_\omega = \bar{\boldsymbol{\omega}}^b - \mathbf{n}_\omega, \end{aligned} \tag{17}$$

where $\bar{\mathbf{a}}^b = \mathbf{a}^b_m - \mathbf{b}_a$ and $\bar{\boldsymbol{\omega}}^b = \boldsymbol{\omega}^b_m - \mathbf{b}_\omega$ are bias corrected acceleration and angular rate vectors, respectively.

$\mathbf{a}^b$ and $\boldsymbol{\omega}^b$ are true acceleration and angular rate of the vehicle. $\mathbf{a}^b_m$ and ω^b_m are measured acceleration and angular rate from the IMU. $\mathbf{n}_a$ and $\mathbf{n}_\omega$ are the IMU acceleration and gyro rate measurement noise terms which are assumed to be zero-mean, white Gaussian noises.
By substituting Eq. (14)$\sim$(17) into Eq. (7), velocity navigation equation becomes

$$\dot{\mathbf{v}}^n = \mathbf{C}^n_b(\mathbf{q}) \ \mathbf{a}^b_{cg} + \mathbf{g}^n = \mathbf{C}^n_b(\mathbf{q}) \ \left(\mathbf{a}^b - \Delta\mathbf{a}^b_{imu}\right) + \mathbf{g}^n = \mathbf{C}^n_b(\mathbf{q}) \ \left(\bar{\mathbf{a}}^b - \Delta\bar{\mathbf{a}}^b_{imu}\right) + \mathbf{g}^n - \mathbf{C}^n_b(\mathbf{q}) \ \mathbf{n}_a, \tag{18}$$

where

$$\Delta\bar{\mathbf{a}}^b_{imu} \cong \dot{\bar{\boldsymbol{\omega}}}^b \times \mathbf{r}^b_{imu} + \bar{\boldsymbol{\omega}}^b \times \left(\bar{\boldsymbol{\omega}}^b \times \mathbf{r}^b_{imu}\right). \tag{19}$$

For the approximation of acceleration correction, $\Delta\bar{\mathbf{a}}^b_{imu}$, of IMU position offset from center of gravity, bias corrected angular rate, $\bar{\boldsymbol{\omega}}^b$, and bias corrected angular acceleration, $\dot{\bar{\boldsymbol{\omega}}}^b$, are used.

By substituting Eq. (17) into Eq. (8), attitude equation becomes

$$\dot{\mathbf{q}} = \frac{1}{2}\boldsymbol{\Omega}(\boldsymbol{\omega}^b)\ \mathbf{q} = \frac{1}{2}\mathbf{Z}(\mathbf{q})\ \boldsymbol{\omega}^b = \frac{1}{2}\boldsymbol{\Omega}(\bar{\boldsymbol{\omega}}^b)\ \mathbf{q} - \frac{1}{2}\mathbf{Z}(\mathbf{q})\ \mathbf{n}_\omega. \tag{20}$$

Here, we used the following relation:

$$\boldsymbol{\Omega}(\mathbf{x})\ \mathbf{q} = \mathbf{Z}(\mathbf{q})\ \mathbf{x}, \text{ for any vector } \mathbf{x} \in R^{3\times 1}. \tag{21}$$

In order to provide more fidelity on the accelerometer and rate gyro error models, time varying dynamics for acceleration biases and rate gyro biases are introduced. The biases are modeled as random walks with zero mean Gaussian driving terms in both the acceleration and rate gyro measurements.

$$\dot{\mathbf{b}}_a = \mathbf{n}_{b_a}, \tag{22}$$

$$\dot{\mathbf{b}}_\omega = \mathbf{n}_{b_\omega}, \tag{23}$$

where $\mathbf{n}_{b_a}$ and $\mathbf{n}_{b_\omega}$ are accelerometer and rate gyro bias noises which are considered to be zero-mean, white Gaussian noises.

Since we are interested in the sensor characteristics of low cost MEMS based IMUs such as the one used in the avionics of autonomous research UAV flight GNC system,[18,6] the accelerations and angular rates usually include large bias and scale factor errors. The scale factor effect can be considered as extra independent states[23,10] or it can be included in the time-varying bias term that is sometimes reasonable assumption[11,5] adopted in our research. Because of the time varying bias effects, additional six states, three for acceleration bias errors and three for rate gyro bias errors, are needed for augmenting the state vector. Now, if we gather the position navigation equation (Eq. (6)), the velocity navigation equation (Eq. (18)), the attitude equation (Eq. (20)), the acceleration bias equation (Eq. (22)), and the rate gyro bias equation (Eq. (23)), we have the following INS navigation process model in continue-time state-space form:

$$\dot{\mathbf{x}}(t) = \mathbf{f}(\mathbf{x}(t)) + \mathbf{G}(\mathbf{x}(t), t)\ \mathbf{w}(t) \tag{24}$$

or

$$\begin{bmatrix} \dot{\mathbf{r}}^n \\ \dot{\mathbf{v}}^n \\ \dot{\mathbf{q}} \\ \dot{\mathbf{b}}_a \\ \dot{\mathbf{b}}_\omega \end{bmatrix} = \begin{bmatrix} \mathbf{v}^n \\ \mathbf{C}^n_b(\mathbf{q})\ (\ \bar{\mathbf{a}}^b - \Delta\bar{\mathbf{a}}^b_{imu}\ ) + \mathbf{g}^n \\ \frac{1}{2}\boldsymbol{\Omega}(\bar{\boldsymbol{\omega}}^b)\mathbf{q} \\ \mathbf{O}_{3\times 1} \\ \mathbf{O}_{3\times 1} \end{bmatrix} + \begin{bmatrix} \mathbf{I}_{3\times 3} & \mathbf{O}_{3\times 3} & \mathbf{O}_{3\times 3} & \mathbf{O}_{3\times 3} & \mathbf{O}_{3\times 3} \\ \mathbf{O}_{3\times 3} & -\mathbf{C}^n_b(\mathbf{q}) & \mathbf{O}_{3\times 3} & \mathbf{O}_{3\times 3} & \mathbf{O}_{3\times 3} \\ \mathbf{O}_{4\times 3} & \mathbf{O}_{4\times 3} & -\frac{1}{2}\mathbf{Z}(\mathbf{q}) & \mathbf{O}_{4\times 3} & \mathbf{O}_{4\times 3} \\ \mathbf{O}_{3\times 3} & \mathbf{O}_{3\times 3} & \mathbf{O}_{3\times 3} & \mathbf{I}_{3\times 3} & \mathbf{O}_{3\times 3} \\ \mathbf{O}_{3\times 3} & \mathbf{O}_{3\times 3} & \mathbf{O}_{3\times 3} & \mathbf{O}_{3\times 3} & \mathbf{I}_{3\times 3} \end{bmatrix} \begin{bmatrix} \mathbf{n}_r \\ \mathbf{n}_a \\ \mathbf{n}_\omega \\ \mathbf{n}_{b_a} \\ \mathbf{n}_{b_\omega} \end{bmatrix}, \tag{25}$$

where

$$\Delta\bar{\mathbf{a}}^b_{imu} = \dot{\bar{\boldsymbol{\omega}}}^b \times \mathbf{r}^b_{imu} + \bar{\boldsymbol{\omega}}^b \times \left(\bar{\boldsymbol{\omega}}^b \times \mathbf{r}^b_{imu}\right) = \begin{bmatrix} \dot{\bar{\omega}}_2 z_a - \dot{\bar{\omega}}_3 y_a + \bar{\omega}_1\left(\bar{\omega}_2 y_a + \bar{\omega}_3 z_a\right) - x_a\left(\bar{\omega}_2^2 + \bar{\omega}_3^2\right) \\ \dot{\bar{\omega}}_3 x_a - \dot{\bar{\omega}}_1 z_a + \bar{\omega}_2\left(\bar{\omega}_1 x_a + \bar{\omega}_3 z_a\right) - y_a\left(\bar{\omega}_1^2 + \bar{\omega}_3^2\right) \\ \dot{\bar{\omega}}_1 y_a - \dot{\bar{\omega}}_2 x_a + \bar{\omega}_3\left(\bar{\omega}_1 x_a + \bar{\omega}_2 y_a\right) - z_a\left(\bar{\omega}_1^2 + \bar{\omega}_2^2\right) \end{bmatrix}, \tag{26}$$

$$\bar{\mathbf{a}}^b = \mathbf{a}^b_m - \mathbf{b}_a = [\ \bar{a}_1\ \bar{a}_2\ \bar{a}_3\ ]^T, \tag{27}$$

$$\bar{\boldsymbol{\omega}}^b = \boldsymbol{\omega}^b_m - \mathbf{b}_\omega = [\ \bar{\omega}_1\ \bar{\omega}_2\ \bar{\omega}_3\ ]^T. \tag{28}$$

The state vector of the process model in the INS process model is defined to include three position components, three velocity components, four quaternion components, three acceleration biases, and three angular rate biases:

$$\mathbf{x} = \begin{bmatrix} \mathbf{r}^n \\ \mathbf{v}^n \\ \mathbf{q} \\ \mathbf{b}_a \\ \mathbf{b}_\omega \end{bmatrix}, \text{ where } \mathbf{r}^n = \begin{bmatrix} X \\ Y \\ Z \end{bmatrix}, \mathbf{v}^n = \begin{bmatrix} U \\ V \\ W \end{bmatrix}, \mathbf{q} = \begin{bmatrix} q_0 \\ q_1 \\ q_2 \\ q_3 \end{bmatrix}, \mathbf{b}_a = \begin{bmatrix} a_{bx} \\ a_{by} \\ a_{bz} \end{bmatrix}, \mathbf{b}_\omega = \begin{bmatrix} \omega_{bx} \\ \omega_{by} \\ \omega_{bz} \end{bmatrix}. \tag{29}$$

Here, $\mathbf{r}^n$ and $\mathbf{v}^n$ are position and velocity vector of the vehicle in the navigation frame, respectively. $\mathbf{q}$ is quaternion vector that expresses the vehicle attitude. $\mathbf{b}_a$ and $\mathbf{b}_\omega$ are IMU acceleration bias vector and IMU rate gyro bias vector, respectively. $\mathbf{n}_r$ is a fictitious zero-mean, white noise associated to the position navigation equation.

In order to apply EKF to continuous-time process model, we need to calculate the following Jacobian matrix from the nonlinear system in Eq. (24) $\sim$ (28):

$$\mathbf{F}_k = \frac{\partial \mathbf{f}}{\partial \mathbf{x}}|_{\mathbf{x}=\mathbf{x}_k} = \begin{bmatrix} \mathbf{O}_{3\times3} & \mathbf{I}_{3\times3} & \mathbf{O}_{3\times4} & \mathbf{O}_{3\times3} & \mathbf{O}_{3\times3} \\ \mathbf{O}_{3\times3} & \mathbf{O}_{3\times3} & \left(\frac{\partial \mathbf{f}_v}{\partial \mathbf{q}}\right)_{3\times4} & \left(\frac{\partial \mathbf{f}_v}{\partial \mathbf{b}_a}\right)_{3\times3} & \mathbf{O}_{3\times3} \\ \mathbf{O}_{4\times3} & \mathbf{O}_{4\times3} & \left(\frac{\partial \mathbf{f}_q}{\partial \mathbf{q}}\right)_{4\times4} & \mathbf{O}_{4\times3} & \left(\frac{\partial \mathbf{f}_q}{\partial \mathbf{b}_\omega}\right)_{4\times3} \\ \mathbf{O}_{3\times3} & \mathbf{O}_{3\times3} & \mathbf{O}_{3\times4} & \mathbf{O}_{3\times3} & \mathbf{O}_{3\times3} \\ \mathbf{O}_{3\times3} & \mathbf{O}_{3\times3} & \mathbf{O}_{3\times4} & \mathbf{O}_{3\times3} & \mathbf{O}_{3\times3} \end{bmatrix}_k, \tag{30}$$

where

$$\begin{aligned}
&\left(\frac{\partial \mathbf{f}_v}{\partial \mathbf{q}}\right)_{3\times4} \\
&= \begin{bmatrix} 2(-q_3\bar{a}_2 + q_2\bar{a}_3) & 2(q_2\bar{a}_2 + q_3\bar{a}_3) & 2(-2q_2\bar{a}_1 + q_1\bar{a}_2 + q_0\bar{a}_3) & 2(-2q_3\bar{a}_1 - q_0\bar{a}_2 + q_1\bar{a}_3) \\ 2(q_3\bar{a}_1 - q_1\bar{a}_3) & 2(q_2\bar{a}_1 - 2q_1\bar{a}_2 - q_0\bar{a}_3) & 2(q_1\bar{a}_1 + q_3\bar{a}_3) & 2(q_0\bar{a}_1 - 2q_3\bar{a}_2 + q_2\bar{a}_3) \\ 2(-q_2\bar{a}_1 + q_1\bar{a}_2) & 2(q_3\bar{a}_1 + q_0\bar{a}_2 - 2q_1\bar{a}_3) & 2(-q_0\bar{a}_1 + q_3\bar{a}_2 - 2q_2\bar{a}_3) & 2(q_1\bar{a}_1 + q_2\bar{a}_2) \end{bmatrix}, \\
&\left(\frac{\partial \mathbf{f}_v}{\partial \mathbf{b}_a}\right)_{3\times3} = -\mathbf{C}_b^n(\mathbf{q}), \\
&\left(\frac{\partial \mathbf{f}_q}{\partial \mathbf{q}}\right)_{4\times4} = \frac{1}{2}\mathbf{\Omega}(\bar{\boldsymbol{\omega}}^b), \\
&\left(\frac{\partial \mathbf{f}_q}{\partial \mathbf{b}_\omega}\right)_{4\times3} = -\frac{1}{2}\mathbf{Z}(\mathbf{q}).
\end{aligned} \tag{31}$$

Note that the IMU offset effect from vehicle center of gravity, $\Delta\bar{\mathbf{a}}^b_{imu}$, and gravity change due to vehicle position, $\mathbf{g}^n$, are neglected in the calculation of Jacobian matrix, $\mathbf{F}_k$.

B. Discrete Process Model of INS Navigation

We need discrete time process model in order to apply unscented Kalman filter. The discrete time model of the continuous time process model in Eq. (24) $\sim$ (28) can be approximated by the following first-order Euler integration algorithm:

$$\mathbf{r}^n_{k+1} = \mathbf{p}^n_k + \dot{\mathbf{r}}^n_k\,\Delta t = \mathbf{r}^n_k + \mathbf{v}^n_k\,\Delta t \tag{32}$$

$$\mathbf{v}^n_{k+1} = \mathbf{v}^n_k + \dot{\mathbf{v}}^n_k\,\Delta t = \mathbf{v}^n_k + \left[\ \mathbf{C}^n_b(\mathbf{q}_k)\ (\ \bar{\mathbf{a}}^b_k - \Delta\bar{\mathbf{a}}^b_{imu,k}\ ) + \mathbf{g}^n\ \right]\Delta t\ -\ \Delta t\ \mathbf{C}^n_b(\mathbf{q}_k)\ \mathbf{n}_{a,k} \tag{33}$$

$$\begin{aligned}
\mathbf{q}_{k+1} &= \mathbf{q}^{\frac{1}{2}\mathbf{\Omega}(\boldsymbol{\omega}^b_k)\,\Delta t}\,\mathbf{q}_k \simeq \left[\ \mathbf{I}_{4\times4} + \frac{1}{2}\mathbf{\Omega}(\boldsymbol{\omega}^b_k)\,\Delta t\ \right]\ \mathbf{q}_k = \left[\ \mathbf{I}_{4\times4} + \frac{1}{2}\mathbf{\Omega}(\bar{\boldsymbol{\omega}}^b_k - \mathbf{n}_{\omega,k})\,\Delta t\ \right]\ \mathbf{q}_k \\
&= \left[\ \mathbf{I}_{4\times4} + \frac{1}{2}\mathbf{\Omega}(\bar{\boldsymbol{\omega}}^b_k)\,\Delta t\ \right]\ \mathbf{q}_k - \frac{\Delta t}{2}\ \mathbf{\Omega}(\mathbf{n}_{\omega,k})\mathbf{q}_k \\
&= \left[\ \mathbf{I}_{4\times4} + \frac{1}{2}\mathbf{\Omega}(\bar{\boldsymbol{\omega}}^b_k)\,\Delta t\ \right]\ \mathbf{q}_k - \frac{\Delta t}{2}\ \mathbf{Z}(\mathbf{q}_k)\ \mathbf{n}_{\omega,k} \\
&\quad (\ \because \mathbf{\Omega}(\mathbf{x})\ \mathbf{q} = \mathbf{Z}(\mathbf{q})\ \mathbf{x} \text{ for any } \mathbf{x} \in R^{3\times1}\ )
\end{aligned} \tag{34}$$

$$\mathbf{b}_{a,k+1} = \mathbf{b}_{a,k} + \mathbf{n}_{b_a,k}\,\Delta t \tag{35}$$

$$\mathbf{b}_{\omega,k+1} = \mathbf{b}_{\omega,k} + \mathbf{n}_{b_\omega,k}\,\Delta t \tag{36}$$

If we gather above equations in matrix form with the noise terms separately, we have the following approximate discrete nonlinear equation for INS navigation process model.

$$\mathbf{x}_{k+1} = \mathbf{f}_d(\mathbf{x}_k, k) + \mathbf{G}_k\ \mathbf{w}_k \tag{37}$$

or

$$\begin{aligned}\begin{bmatrix} \mathbf{r}^n_{k+1} \\ \mathbf{v}^n_{k+1} \\ \mathbf{q}_{k+1} \\ \mathbf{b}_{a,k+1} \\ \mathbf{b}_{\omega,k+1} \end{bmatrix} &= \begin{bmatrix} \mathbf{r}^n_k + \mathbf{v}^n_k\ \Delta t \\ \mathbf{v}^n_k + \left[\ \mathbf{C}^n_b(\mathbf{q}_k)\ (\ \bar{\mathbf{a}}^b_k - \Delta\bar{\mathbf{a}}^b_{imu,k}\ ) + \mathbf{g}^n\ \right] \Delta t \\ \left[\ \mathbf{I}_{4\times4} + \frac{1}{2}\mathbf{\Omega}(\bar{\boldsymbol{\omega}}^b_k)\ \Delta t\ \right]\ \mathbf{q}_k \\ \mathbf{b}_{a,k} \\ \mathbf{b}_{\omega,k} \end{bmatrix} \\ &+ \begin{bmatrix} \Delta t\ \mathbf{I}_{3\times3} & \mathbf{O}_{3\times3} & \mathbf{O}_{3\times3} & \mathbf{O}_{3\times3} & \mathbf{O}_{3\times3} \\ \mathbf{O}_{3\times3} & -\Delta t\ \mathbf{C}^n_b(\mathbf{q}_k) & \mathbf{O}_{3\times3} & \mathbf{O}_{3\times3} & \mathbf{O}_{3\times3} \\ \mathbf{O}_{4\times3} & \mathbf{O}_{4\times3} & -\frac{\Delta t}{2}\mathbf{Z}(\mathbf{q}_k) & \mathbf{O}_{4\times3} & \mathbf{O}_{4\times3} \\ \mathbf{O}_{3\times3} & \mathbf{O}_{3\times3} & \mathbf{O}_{3\times3} & \Delta t\ \mathbf{I}_{3\times3} & \mathbf{O}_{3\times3} \\ \mathbf{O}_{3\times3} & \mathbf{O}_{3\times3} & \mathbf{O}_{3\times3} & \mathbf{O}_{3\times3} & \Delta t\ \mathbf{I}_{3\times3} \end{bmatrix} \begin{bmatrix} \mathbf{n}_{r,k} \\ \mathbf{n}_{a,k} \\ \mathbf{n}_{\omega,k} \\ \mathbf{n}_{b_a,k} \\ \mathbf{n}_{b_\omega,k} \end{bmatrix} \end{aligned} \tag{38}$$

where
$\bar{\mathbf{a}}^b_k = \mathbf{a}^b_{m,k} - \mathbf{b}_{a,k}$ and $\bar{\boldsymbol{\omega}}^b_k = \boldsymbol{\omega}^b_{m,k} - \mathbf{b}_{\omega,k}$ are bias corrected IMU accelerometer and rate gyro measurements.

III. INS Navigation Measurement Model

In order to compensate the data degradation of low-cost IMU with time, integrated navigation system that combines low-cost IMU with aiding sensors is designed. our autonomous research UAV is equipped with the following IMU and aiding sensors.[18, 19, 6, 16]

- Inertial Sciences ISIS-IMU : three axis acceleration and angular rates
- NovAtel Millenium RT-2 Differential GPS receiver : inertial position and velocity
- Honeywell HMR-2300R Magnetometer : heading information
- Vision sensor : relative target position

Sensor update rates are summarized in table 1.

Table 1. Sensor Update Rates

Sensor	Update rate	Measurements
IMU	100 Hz	vehicle acceleration & angular rates
DGPS	5 Hz	inertial position & velocity
Magnetometer	20 Hz	heading information
Vision sensor	10 Hz	relative target position

Using the high frequency vehicle accelerations and angular rates, inertial navigation mechanization algorithm can provide high rate vehicle position/velocity and attitude that are necessary for autonomous UAV flight GNC system. Because of IMU measurement errors, errors in the estimates of vehicle position/velocity and attitude grow with time. In order to compensate this long term errors, aiding sensors such as DGPS, Magnetometer, altimeter, and so on are generally equipped in addition to IMU. These aiding sensors measure data in relatively low frequency but obtain time independent accurate data. IMU can provide complete navigation information such as vehicle position/velocity and attitude, while IMU-measured accelerations and angular rates need to be time-integrated to get these navigation information. On the other hand, aiding sensors usually provide only part of navigation information, but it can be directly used to get navigation information without involvement of dynamic equations.

Since IMU measurement rate is relatively higher than other aiding sensors, IMU measurements are considered to be continuous data flow. IMU measured vehicle accelerations and angular rates are treated as the inputs to the process model.

Since aiding sensors have several different update rates, we need to carefully treat measurement updates in Kalman filtering framework. Due to the variation in the number of available measurements depending on time instant, the dimensions of measurement vector and Kalman gain matrix are highly varying. In order to easily deal with this multi-rate sensor fusion problem, we apply the "sequential processing of measurement updates" method.[24,5,25] In this approach, measurement updates are not considered in a whole and in a big measurement matrix/vector, but rather each measurement is treated separately, sequentially, and in small-size several vectors/matrices. The addition of new aiding sensors is easier in this framework than in the standard Kalman filtering framework. Keeping this argument in mind, separate measurement model for each aiding sensors are described in this section. Vision sensor information is also considered as another source of independent measurement and treated within this framework of sequential measurement update. The details of vision sensor measurement model are presented in related references and thus excluded from this paper.[26,27]

A. DGPS Position and Velocity Measurement Model

Since the position and velocity of INS output are degraded in time, GPS receiver is augmented to frequently update the vehicle position and velocity in navigation frame and to correct the long term INS errors. The selected DGPS receiver provides position and velocity information at a slower rate compared to INS system. Since the GPS antenna is mounted off the vehicle's center of gravity, DGPS sensor measures the position and velocity at the GPS mounting location with respect to the center of gravity, $\mathbf{r}^b_{gps}$. Furthermore, GPS measurements have a latency and need to be compensated. Considering this GPS latency, current position/velocity measurements are actually previous position/velocity and current updates are based on older state estimate corresponding to this latency. In our integrated INS navigation, GPS position and velocity have different latency and their measurement updates are applied independently.

$$\mathbf{y}^1_k = \mathbf{h}^1(\mathbf{x}_k) + \mathbf{n}^{gps}_{r,k} \quad \Leftrightarrow \quad \mathbf{r}^{gps}_k = \mathbf{r}^n_{k-L1} + \mathbf{C}^n_b(\mathbf{q}_{k-L1})\,\mathbf{r}^b_{gps} + \mathbf{n}^{gps}_{r,k}, \tag{39}$$

$$\mathbf{y}^2_k = \mathbf{h}^2(\mathbf{x}_k) + \mathbf{n}^{gps}_{v,k} \quad \Leftrightarrow \quad \mathbf{v}^{gps}_k = \mathbf{v}^n_{k-L2} + \mathbf{C}^n_b(\mathbf{q}_{k-L2})\,\bar{\boldsymbol{\omega}}^b_{k-L2} \times \mathbf{r}^b_{gps} + \mathbf{n}^{gps}_{v,k}, \tag{40}$$

where $\mathbf{r}^n_{k-L1}$ and $\mathbf{v}^n_{k-L2}$ are the time-delayed vehicle position and vehicle velocity vector in the navigation frame. $\bar{\boldsymbol{\omega}}_{k-L2}$ is the time-delayed vehicle angular rate vector in the body frame. Time delay comes from the GPS sensor latency and $L_1 = \frac{GPS\ position\ latency}{\Delta t}$ and $L_2 = \frac{GPS\ velocity\ latency}{\Delta t}$. $\mathbf{r}^b_{gps}$ is the location of the GPS antenna relative to vehicle's center of gravity location in the body frame.

$$\mathbf{H}^1 = \frac{\partial \mathbf{h}^1}{\partial \mathbf{x}} = \left[\left(\frac{\partial \mathbf{h}^1}{\partial \mathbf{r}^n}\right)_{3\times3} \quad \mathbf{O}_{3\times3} \quad \left(\frac{\partial \mathbf{h}^1}{\partial \mathbf{q}}\right)_{3\times4} \quad \mathbf{O}_{3\times3} \quad \mathbf{O}_{3\times3}\right], \tag{41}$$

$$\mathbf{H}^2 = \frac{\partial \mathbf{h}^2}{\partial \mathbf{x}} = \left[\mathbf{O}_{3\times3} \quad \left(\frac{\partial \mathbf{h}^2}{\partial \mathbf{v}^n}\right)_{3\times3} \quad \left(\frac{\partial \mathbf{h}^2}{\partial \mathbf{q}}\right)_{3\times4} \quad \mathbf{O}_{3\times3} \quad \left(\frac{\partial \mathbf{h}^2}{\partial \mathbf{b}_\omega}\right)_{3\times3}\right], \tag{42}$$

where

$$\left(\frac{\partial \mathbf{h}^1}{\partial \mathbf{r}^n}\right)_{3\times3} = \mathbf{I}_{3\times3}, \quad \left(\frac{\partial \mathbf{h}^2}{\partial \mathbf{v}^n}\right)_{3\times3} = \mathbf{I}_{3\times3}, \tag{43}$$

$$\left(\frac{\partial \mathbf{h}^2}{\partial \mathbf{q}}\right)_{3\times4} = \mathbf{O}_{3\times4}, \quad \left(\frac{\partial \mathbf{h}^2}{\partial \mathbf{b}_\omega}\right)_{3\times3} = \mathbf{O}_{3\times3}, \tag{44}$$

$$\left(\frac{\partial \mathbf{h}^1}{\partial \mathbf{q}}\right)_{3\times4} = \begin{bmatrix} 2(-q_3y_g + q_2z_g) & 2(q_2y_g + q_3z_g) & 2(-2q_2x_g + q_1y_g + q_0z_g) & 2(-2q_3x_g - q_0y_g + q_1z_g) \\ 2(q_3x_g - q_1z_g) & 2(q_2x_g - 2q_1y_g - q_0z_g) & 2(q_1x_g + q_3z_g) & 2(q_0x_g - 2q_3y_g + q_2z_g) \\ 2(-q_2x_g + q_1y_g) & 2(q_3x_g + q_0y_g - 2q_1z_g) & 2(-2q_0x_g + q_3y_g - 2q_2z_g) & 2(q_1x_g + q_2y_g) \end{bmatrix}. \tag{45}$$

Note that quaternion effect and angular rate bias effect are approximated to be negligible in the Jacobian computation of GPS velocity measurement.

B. Magnetometer Measurement Model

Three axes magnetometer measures Earth magnetic field line in body frame. The measured Earth magnetic field vector is used to correct for heading compensation. The basic idea for yaw angle compensation is as follows. The residual quantity in the measurement of declination angle will be the same as the residual of yaw angle. Hence we first compute the residual value of declination angle instead of that of yaw angle, and then this residual (difference between ideal declination angle given by world magnetic model and measured declination angle) is used to compensate yaw angle in the framework of extended Kalman filter. The following measurement model is used for yaw angle measurement:

$$\mathbf{y}_k^3 = \mathbf{h}^3(\mathbf{x}_k) + \mathbf{n}_\psi \quad \Leftrightarrow \quad \psi = atan2\left(C_{21},\ C_{11}\right) + \mathbf{n}_\psi = atan2\left[2(q_1q_2 + q_0q_3),\ q_0^2 + q_1^2 - q_2^2 - q_3^2\right] + \mathbf{n}_\psi, \quad (46)$$

where ψ is true heading angle and C_{ij} are corresponding components in rotation matrix $\mathbf{C}_b^n$ expressed in (9).

The measurement Jacobian matrix for magnetometer measurement $\mathbf{H}^3$ are computed using these relations.

$$\mathbf{H}^3 = \frac{\partial \mathbf{h}^3}{\partial \mathbf{x}} = \begin{bmatrix} \mathbf{O}_{1\times3} & \mathbf{O}_{1\times3} & \left(\frac{\partial \mathbf{h}^3}{\partial \mathbf{q}}\right)_{1\times4} & \mathbf{O}_{1\times3} & \mathbf{O}_{1\times3} \end{bmatrix}, \quad (47)$$

where

$$\left(\frac{\partial \mathbf{h}^3}{\partial \mathbf{q}}\right)_{1\times4} = \begin{bmatrix} \frac{\partial\psi}{\partial q_0} & \frac{\partial\psi}{\partial q_1} & \frac{\partial\psi}{\partial q_2} & \frac{\partial\psi}{\partial q_3} \end{bmatrix}, \quad (48)$$

$$\frac{\partial\psi}{\partial q_0} = s_x(q_3C_{11} - q_0C_{21}), \quad (49)$$

$$\frac{\partial\psi}{\partial q_1} = s_x(q_2C_{11} - q_1C_{21}), \quad (50)$$

$$\frac{\partial\psi}{\partial q_2} = s_x(q_1C_{11} + q_2C_{21}), \quad (51)$$

$$\frac{\partial\psi}{\partial q_3} = s_x(q_0C_{11} + q_3C_{21}), \quad (52)$$

$$s_x = \frac{2}{(C_{11})^2 + (C_{21})^2}. \quad (53)$$

Note that both the heading angle expression and the measurement Jacobian for magnetometer triad $\mathbf{H}^3$ does not explicitly depend on magnetometer triad. Magnetometer triad are involved in the calculation of yaw angle residual which is used to compensate heading angle. Computation of yaw angle residual will be explained in detail in the next section.

IV. Integrated INS Navigation Using EKF and UKF

In order to fuse aiding sensor measurements with INS navigation algorithm, both extended Kalman filter (EKF) and unscented Kalman filter (UKF) are used. This section describes the sensor fusion architecture and the details of Kalman filter implementation. Figure 2 shows the overall integrated strapdown INS mechanization. Note that only bias effects are considered to be independent states and are used to correct IMU sensor drifts.

The INS outputs are used as a reference trajectory and attitude. Aiding sensor measurements such as vehicle inertial position and velocity from DGPS and heading information from three-axis magnetometer are applied to update the states of these trajectory and attitude, and hence limit the long term error growth with time.

A. Extended Kalman Filter with Sequential Measurement Update

As a reference integrated INS model discussed in detail at the Ref. 6, 16, 17, the extended Kalman filter is applied to the nonlinear continuous-time process model and discrete-time measurement model in state-space form. As explained in the previous section, measurement models are expressed in separate form for each sensor in order to apply the "Sequential processing of Multi-rate measurements".[5, 24, 28]

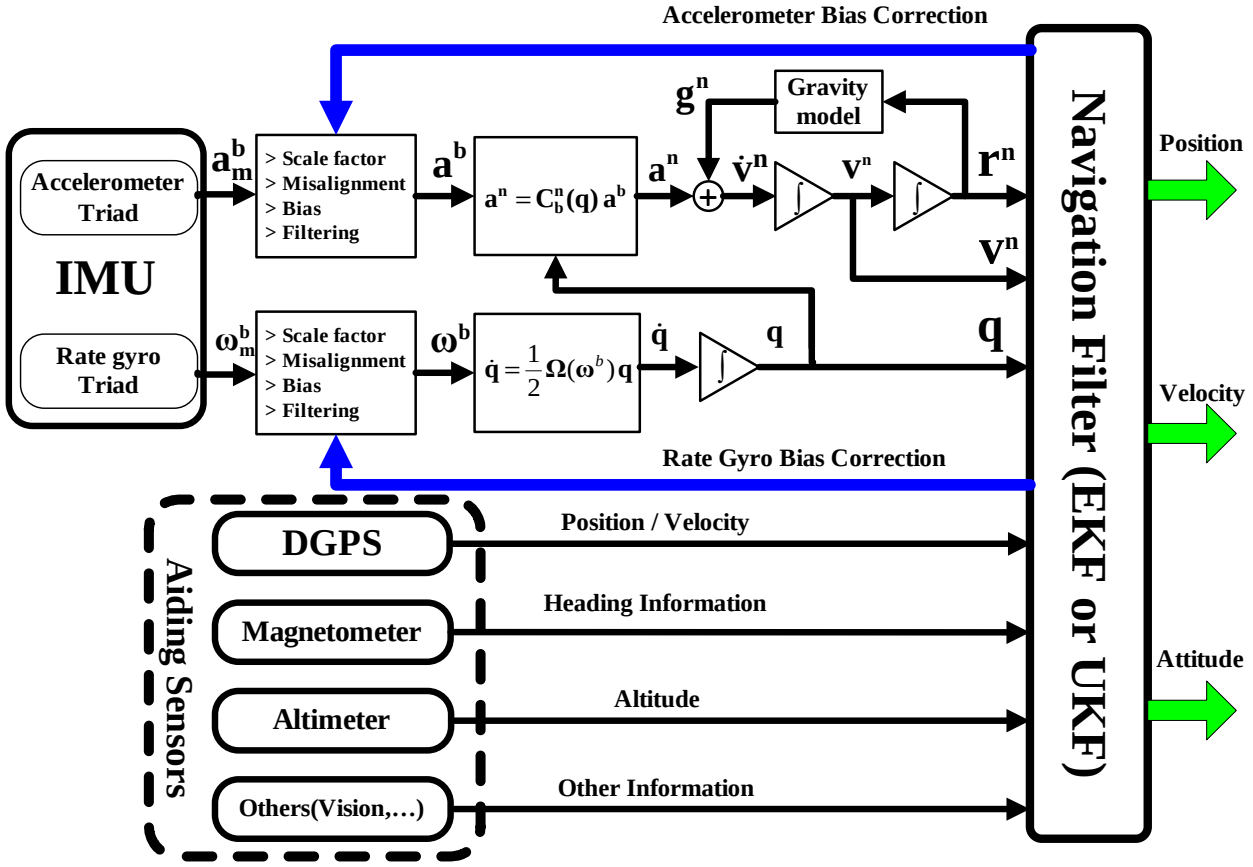

Figure 2. Integrated Strapdown Inertial Navigation System.

The general nonlinear continuous-time process model and discrete-time measurement model in state-space form are given by:

$$\dot{\mathbf{x}}(t) = \mathbf{f}(\mathbf{x}(t), \mathbf{u}(t), t) + \mathbf{G}(\mathbf{x}(t), t)\ \mathbf{w}(t), \qquad \mathbf{w}(t) \sim N(0, \mathbf{Q}(t)), \tag{54}$$

$$\mathbf{y}_k^l = \mathbf{h}^l(\mathbf{x}_k, k) + \mathbf{v}_k^l, \qquad \mathbf{v}_k^l \sim N(0, \mathbf{R}_k^l), \quad l = 1, 2, \cdots, r, \tag{55}$$

where r is the number of aiding sensor measurements.

The initial conditions ($\mathbf{x}(t_0) \sim N(\hat{\mathbf{x}}_0, \mathbf{P}_0)$) are assumed to be known and have the following form:

$$\hat{\mathbf{x}}_0 = E[\mathbf{x}(t_0)], \tag{56}$$

$$\mathbf{P}_0 = E[(\mathbf{x}(t_0) - \hat{\mathbf{x}}_0)(\mathbf{x}(t_0) - \hat{\mathbf{x}}_0)^T]. \tag{57}$$

Jacobians matrices of system dynamics and measurement model are defined as:

$$\mathbf{F}(\hat{\mathbf{x}}(t), t) = \frac{\partial \mathbf{f}}{\partial \mathbf{x}}|_{\mathbf{x}(t)=\hat{\mathbf{x}}(t)}, \tag{58}$$

$$\mathbf{H}_k^l = \frac{\partial \mathbf{h}^l(\mathbf{x}, k)}{\partial \mathbf{x}}|_{\mathbf{x}=\hat{\mathbf{x}}_k^- = \hat{\mathbf{x}}(t_k^-)}, \quad l = 1, 2, \cdots, r. \tag{59}$$

1. Time Update

Given the state estimate $\hat{\mathbf{x}}_{k-1} = \hat{\mathbf{x}}(t_{k-1})$ and error covariance matrix $\mathbf{P}_{k-1} = \mathbf{P}(t_{k-1})$ at time $t = t_{k-1}$, current state estimate $\hat{\mathbf{x}}_k^- = \hat{\mathbf{x}}(t_k^-)$ and error covariance matrix $\mathbf{P}_k^- = \mathbf{P}(t_k^-)$ can be obtained by integrating forward from $t = t_{k-1}$ to $t = t_k^-$ ($k = 1, 2, \cdots$) using the following state estimate propagation equation and

error covariance propagation equation:

$$\dot{\hat{\mathbf{x}}}(t) = \mathbf{f}(\hat{\mathbf{x}}(t), \mathbf{u}(t), t), \tag{60}$$

$$\dot{\mathbf{P}}(t) = \mathbf{F}(\hat{\mathbf{x}}(t), t)\, \mathbf{P}(t) + \mathbf{P}(t)\, \mathbf{F}^T(\hat{\mathbf{x}}(t), t) + \mathbf{G}(\mathbf{x}(t), t)\, \mathbf{Q}(t)\, \mathbf{G}^T(\mathbf{x}(t), t). \tag{61}$$

2. Sequential Measurement Update

Given the time updated state and error covariance matrix $\hat{\mathbf{x}}_k^-, \mathbf{P}_k^-$ with new measurement vector $\mathbf{y}_k = \mathbf{y}(t_k) = \left[\mathbf{y}^1(t_k)^T \cdots \mathbf{y}^r(t_k)^T\right]^T$, we apply the "sequential processing of measurement update" in order to obtain the measurement updated state and error covariance matrix $\hat{\mathbf{x}}_k = \hat{\mathbf{x}}(t_k), \mathbf{P}_k = \mathbf{P}(t_k)$. For each available measurement $\mathbf{y}_k^l = \mathbf{y}^l(t_k)$ $(l = 1, \cdots, r)$ at time instant $t = t_k$, we can update the state estimate $\hat{\mathbf{x}}_k$ and error covariance matrix $\mathbf{P}_k$ by the following sequential measurement processing.

For $l = 1, 2, \cdots, r$ (r measurements update at time $t = t_k$),

$$\mathbf{K}_k^l = \mathbf{P}_k^{l-1}\, \mathbf{H}_k^{l\,T}(\hat{\mathbf{x}}_k^{l-1}) \left[\mathbf{H}_k^l(\hat{\mathbf{x}}_k^{l-1})\, \mathbf{P}_k^{l-1}\, \mathbf{H}_k^{l\,T}(\hat{\mathbf{x}}_k^{l-1}) + \mathbf{R}_k^l\right]^{-1}, \tag{62}$$

$$\hat{\mathbf{x}}_k^l = \hat{\mathbf{x}}_k^{l-1} + \mathbf{K}_k^l \left[\, \mathbf{y}_k^l - \mathbf{h}^l(\hat{\mathbf{x}}_k^{l-1}) \,\right], \tag{63}$$

$$\mathbf{P}_k^l = \left[\mathbf{I} - \mathbf{K}_k^l \mathbf{H}_k^l\right] \mathbf{P}_k^{l-1} \left[\mathbf{I} - \mathbf{K}_k^l \mathbf{H}_k^l\right]^T + \mathbf{K}_k^l \mathbf{R}_k^l \mathbf{K}_k^{l\,T}, \tag{64}$$

$$\left(\mathbf{P}_k^l = \left[\mathbf{I} - \mathbf{K}_k^l \mathbf{H}_k^l\right] \mathbf{P}_k^{l-1} \right), \quad l = 1, 2, \cdots, r, \tag{65}$$

where starting initial condition for this sequential measurement update at $t = t_k^-$ is $\hat{\mathbf{x}}_k^0 = \hat{\mathbf{x}}_k^- = \hat{\mathbf{x}}(t_k^-)$, $\mathbf{P}_k^0 = \mathbf{P}_k^- = \mathbf{P}(t_k^-)$ and final measurement update is set as $\hat{\mathbf{x}}_k = \hat{\mathbf{x}}(t_k) = \hat{\mathbf{x}}_k^r$, $\mathbf{P}_k = \mathbf{P}(t_k) = \mathbf{P}_k^r$.

For every measurement not available at time $t = t_k$, we can skip this measurement update step. Whenever a measurement is available at any time instant $t = t_k$, that measurement can be included for this sequential measurement update processing. For more detailed derivation and theoretical explanation, refer to the Ref. 5, 25.

GPS Measurement Update with Sensor Latency Compensation

In (63), we need to use proper state vector for the calculation of nonlinear measurement model in case where there is sensor latency. Since GPS position and velocity measurement model need to use latency compensated state vector (i.e., previous states depending on corresponding latency), measurement estimate components $\hat{\mathbf{y}}_k^l$, $(l = 1, 2)$ corresponding to GPS position and velocity are computed by using latency compensated states.

$$\hat{\mathbf{x}}_k^l = \hat{\mathbf{x}}_k^{l-1} + \mathbf{K}_k^l \left[\, \mathbf{y}_k^l - \hat{\mathbf{y}}_k^l \,\right], \; l = 1, 2, \tag{66}$$

where

$$\hat{\mathbf{y}}_k^l = \mathbf{h}^l(\hat{\mathbf{x}}_{k-L}^-), \tag{67}$$

and $L = \frac{Aiding\ sensor\ latency}{\Delta t}$ is time delayed steps corresponding to sensor latency ($L = L_1$ for GPS position latency and $L = L_2$ for GPS velocity latency.)

Magnetometer Measurement Update

Three axes magnetometer measures Earth magnetic field line in body frame. The measured Earth magnetic field vector is used to compensate for vehicle heading. Yaw angle measurement update is based on the assumption that the residual in the measurement of declination angle, $\Delta\psi_d$, will be the same as the residual of yaw angle, $\Delta\psi$. Then we can use the residual value of declination angle for the compensation of yaw angle in the extended Kalman filter framework as follows:

$$\hat{\mathbf{x}}_k^l = \hat{\mathbf{x}}_k^{l-1} + \mathbf{K}_k^l \left[\, \mathbf{y}_k^l - \hat{\mathbf{y}}_k^l \,\right], \; l = 3, \tag{68}$$

where

$$\Delta\psi = \Delta\psi_d = \mathbf{y}_k^l - \hat{\mathbf{y}}_k^l, \tag{69}$$

$$\mathbf{y}_k^l = \psi_{d,measure} = atan2\left(h_y^n,\ h_x^n\right), \tag{70}$$

$$\hat{\mathbf{y}}_k^l = \psi_{d,estimate}, . \tag{71}$$

Here, ψ_d is local variation or declination angle that is the angle between true north and magnetic north, and $\psi_{d,estimate}$ is obtained by world magnetic model 2005 (WMM-2005).[29] In addition, $\mathbf{h}^n = [\ h_x^n \quad h_y^n \quad h_z^n\ ]^T$ is magnetic field triad in local navigation frame (NED). This is obtained by projecting the magnetic field vector on the local navigation frame (North-East-Down plane), using the last vehicle attitude estimate $\hat{\mathbf{q}}$, to eliminate the effects of magnetic dip. Since $\mathbf{h}^n = \mathbf{C}_b^n\ \mathbf{h}^b$ and $\mathbf{h}^b = [\ h_x^b \quad h_y^b \quad h_z^b\ ]^T$ are measured from magnetometer triad, we get the relations:

$$h_x^n = h_x^b\ C_{11} + h_y^b\ C_{12} + h_z^b\ C_{13}, \tag{72}$$

$$h_y^n = h_x^b\ C_{21} + h_y^b\ C_{22} + h_z^b\ C_{23}, \tag{73}$$

where C_{ij} are corresponding components in rotation matrix $\mathbf{C}_b^n$ expressed in (9).

3. Implementation

In order to overcome the usual computational power limitation in low-cost UAV onboard system, several efforts are made. At first, we introduced the following noise definitions:

$$\mathbf{n}_v \triangleq -\mathbf{C}_b^n(\mathbf{q})\ \mathbf{n}_a, \tag{74}$$

$$\mathbf{n}_q \triangleq -\frac{1}{2}\mathbf{Z}(\mathbf{q})\ \mathbf{n}_\omega. \tag{75}$$

Then the INS navigation process model in continue-time state-space form becomes as the following rather simple form:

$$\dot{\mathbf{x}}(t) = \mathbf{f}(\mathbf{x}(t)) + \mathbf{w}_1(t) \tag{76}$$

or

$$\begin{bmatrix} \dot{\mathbf{r}}^n \\ \dot{\mathbf{v}}^n \\ \dot{\mathbf{q}} \\ \dot{\mathbf{b}}_a \\ \dot{\mathbf{b}}_\omega \end{bmatrix} = \begin{bmatrix} \mathbf{v}^n \\ \mathbf{C}_b^n(\mathbf{q})\ (\ \bar{\mathbf{a}}^b - \Delta\bar{\mathbf{a}}_{imu}^b\ ) + \mathbf{g}^n \\ \frac{1}{2}\mathbf{\Omega}(\bar{\boldsymbol{\omega}}^b)\mathbf{q} \\ \mathbf{O}_{3\times1} \\ \mathbf{O}_{3\times1} \end{bmatrix} + \begin{bmatrix} \mathbf{n}_r \\ \mathbf{n}_v \\ \mathbf{n}_q \\ \mathbf{n}_{b_a} \\ \mathbf{n}_{b_\omega} \end{bmatrix}. \tag{77}$$

Expressing the INS process model in Eq. (25) is more intuitive as it is represented by direct sensor noises ($\mathbf{n}_a$, $\mathbf{n}_\omega$). The random noise characteristics of accelerometers and rate gyros ($\mathbf{n}_a$, $\mathbf{n}_\omega$) are relatively easily modeled from sensor characteristics and sensor test outputs. On the other hand, the INS process model expressed in Eq. (77) involves difficulty in modeling the noise characteristics of $\mathbf{n}_v$ and $\mathbf{n}_q$ while it has simpler form and thus is computationally more efficient. By using this process model expression, the error covariance propagation equation becomes

$$\dot{\mathbf{P}}(t) = \mathbf{F}(\hat{\mathbf{x}}(t), t)\ \mathbf{P}(t) + \mathbf{P}(t)\ \mathbf{F}^T(\hat{\mathbf{x}}(t), t) + \mathbf{Q}(t), \tag{78}$$

where $\mathbf{Q} = E[\mathbf{w}_1(t)\mathbf{w}_1(t)^T]$ is 16×16 matrix. Comparing the original error covariance propagation equation,

$$\dot{\mathbf{P}}(t) = \mathbf{F}(\hat{\mathbf{x}}(t), t)\ \mathbf{P}(t) + \mathbf{P}(t)\ \mathbf{F}^T(\hat{\mathbf{x}}(t), t) + \mathbf{G}(\mathbf{x}(t), t)\ \mathbf{Q}(t)\ \mathbf{G}^T(\mathbf{x}(t), t), \tag{79}$$

where $\mathbf{Q} = E[\mathbf{w}(t)\mathbf{w}(t)^T]$ is 15×15 matrix, the process model in Eq. (77) contributes in the computational efficiency of navigation filter since it removes 16×15 big matrix $\mathbf{G}(\mathbf{x})$ multiplications. As $\mathbf{n}_v$ is just accelerometer noise in navigation frame and $det(\mathbf{C}_b^n) = 1$ in Eq. (74), statistical characteristics of noise $\mathbf{n}_v$ can be modeled to have the same statistical characteristics of noise $\mathbf{n}_a$. The noise $\mathbf{n}_q$ in $\dot{\mathbf{q}}$ equation is more difficult to

characterize. Since $\mathbf{Z}$ matrix is composed of quaternions that have values lower than 1, the statistical characteristics of noise $\mathbf{n}_q$ can be approximately determined based on those of noise $\mathbf{n}_\omega$ and have been tuned through flight tests. The process noise covariance matrix $\mathbf{Q}$ in current filter is $\mathbf{Q} = diag[\mathbf{Q}_{n_r}, \mathbf{Q}_{n_v}, \mathbf{Q}_{n_q}, \mathbf{Q}_{n_{b_a}}, \mathbf{Q}_{n_{b_\omega}}]$ = diag[0.0 $(ft/s)^2$, 0.0 $(ft/s)^2$, 0.0 $(ft/s)^2$, 0.01 $(ft/s^2)^2$, 0.01 $(ft/s^2)^2$, 0.01 $(ft/s^2)^2$, 0.0001, 0.0001, 0.0001, 0.0001, 0.001 $(ft/s^2)^2$, 0.001 $(ft/s^2)^2$, 0.001 $(ft/s^2)^2$, 0.00001 $(rad/s)^2$, 0.00001 $(rad/s)^2$, 0.00001 $(rad/s)^2$].

The measurement noise covariance matrix of GPS position $\mathbf{R}_{gpsPos} = diag[25^2, 25^2, 30^2]\ ft^2$. Similarly, the measurement noise covariance matrix of GPS velocity $\mathbf{R}_{gpsVel} = diag[10^2, 10^2, 15^2]\ ft^2$. The measurement noise covariance matrix of magnetometer $\mathbf{R}_{mag} = 10^2\ deg^2$.

In the implementation of time update in Eqs. (60) and (61), state estimate is integrated with Runge-Kutta 2nd order algorithm and error covariance matrix is updated using first-order Euler integration algorithm:

$$\hat{\mathbf{x}}_k^- = \int_{t_{k-1}}^{t_k^-} \mathbf{f}(\hat{\mathbf{x}}(t), \mathbf{u}(t), t)\ dt, \tag{80}$$

$$\mathbf{P}_k^- = \mathbf{P}_{k-1} + \Delta t\ \left[\mathbf{F}(\hat{\mathbf{x}}(t_{k-1}), t_{k-1})\ \mathbf{P}(t_{k-1}) + \mathbf{P}(t_{k-1})\ \mathbf{F}^T(\hat{\mathbf{x}}(t_{k-1}), t_{k-1}) + \mathbf{Q}(t_{k-1})\right]. \tag{81}$$

One more thing worth to mention is about the advantage of sequential measurement update. Aiding sensors in INS mechanization are usually not correlated each other and hence sequential measurement update is possible. In this case, measurement update is computationally efficient since series of smaller matrix inversion is involved instead of one big matrix inversion in Eq. (64). Since aiding sensors have several different update rates, we need to carefully treat measurement updates in Kalman filtering framework. Due to the variation in the number of available measurements depending on time instant, the dimensions of measurement vector and Kalman gain matrix are also varying. Sequential measurement update approach is easier to deal with this multi-rate sensor fusion problem. Furthermore, the addition of new aiding sensors in current design is easier in this framework than in the standard Kalman filtering framework.

B. Unscented Kalman Filter with Sequential Measurement Update

The original unscented Kalman filter was first developed by Julier et al.[30,14,31] and further narrowed down by Merwe et al.[11,15,32] in several algorithms. This section introduces the unscented Kalman filter with sequential measurement update. The idea behind this is to recursively update the state estimate and error covariance matrix by using more accurate nonlinear filtering approach, unscented Kalman filter, while keeping the advantages of sequential measurement updates mentioned in the previous sections. By using a new UKF with sequential measurement update instead of standard UKF algorithm, we can keep the advantages of the EKF with sequential measurement update. We can easily handle the multi-rate sensor fusion problem and sensor latency compensation. The addition of new aiding sensors is easier in this framework than in the standard UKF framework. Furthermore, we can remove the messy Jacobian matrices computation and keep at least second-order nonlinear function approximation.

The general nonlinear discrete-time process model and discrete-time measurement model in state-space form are given by:

$$\mathbf{x}_{k+1} = \mathbf{f}_d(\mathbf{x}_k, \mathbf{u}_k, k) + \mathbf{w}_k, \qquad \mathbf{w}_k \sim N(0, \mathbf{Q}_k), \tag{82}$$

$$\mathbf{y}_k^l = \mathbf{h}^l(\mathbf{x}_k, k) + \mathbf{v}_k^l, \qquad \mathbf{v}_k^l \sim N(0, \mathbf{R}_k^l),\ \ l = 1, 2, \cdots, r, \tag{83}$$

where initial conditions ($\mathbf{x}(t_0) \sim N(\hat{\mathbf{x}}_0, \mathbf{P}_0)$) are assumed to be known and r is the number of aiding sensor measurements.

1. Time Update

For each time step $k = 1, 2, \cdots$, we need first to calculate sigma points and then time-update using time-update equations.

• **Sigma-point calculation**

$$\mathbf{S}_{k-1} = \{chol(\mathbf{P}_{k-1})\}^T, \tag{84}$$

$$\mathbf{X}_{k-1} = [\ \hat{\mathbf{x}}_{k-1} \quad \hat{\mathbf{x}}_{k-1} + \gamma\ \mathbf{S}_{k-1} \quad \hat{\mathbf{x}}_{k-1} - \gamma\ \mathbf{S}_{k-1}\ ], \tag{85}$$

where $\mathbf{S}$ is Cholesky factorization of $\mathbf{P}$ in lower triangular matrix form and the constant γ is a parameter to control the dispersion distance from mean estimate in the computation of sigma point matrix $\mathbf{X}$.

• **Time-update equations**

$$\mathbf{X}^*_{k|k-1} = \mathbf{f}_d(\mathbf{X}_{k-1}, \mathbf{u}_{k-1}), \tag{86}$$

$$\hat{\mathbf{x}}^-_k = \sum_{i=0}^{2n} w_i^{(m)} \mathbf{X}^*_{i,k|k-1} \texttt{ with quaternion normalization}, \tag{87}$$

$$\mathbf{P}^-_k = \sum_{i=0}^{2n} w_i^{(c)} (\mathbf{X}^*_{i,k|k-1} - \hat{\mathbf{x}}^-_k)(\mathbf{X}^*_{i,k|k-1} - \hat{\mathbf{x}}^-_k)^T + \mathbf{Q}_k, \tag{88}$$

where $\mathbf{Q}_k = \Delta t\ \mathbf{Q}(t)$.

2. Sequential Measurement Update at time instant ($t = t_k$)

For each available measurement $\mathbf{y}^l_k = \mathbf{y}^l(t_k)$ $(l = 1, \cdots, r)$ at time instant $t = t_k$, we can update the state estimate $\hat{\mathbf{x}}_k$ and error covariance matrix $\mathbf{P}_k$ by the following sequential measurement processing. We choose the time update quantity as initial conditions for measurement update and then process the available measurements sequentially or one by one.
Let the initial conditions be $\hat{\mathbf{x}}^0_k = \hat{\mathbf{x}}^-_k$, $\mathbf{P}^0_k = \mathbf{P}^-_k$ and iterate measurement update loop for $l = 1, 2, \cdots, r$ (r measurement updates at time $t = t_k$).

• **Augmented sigma points**

$$\mathbf{S}^{l-1}_k = \sqrt{\mathbf{P}^{l-1}_k} = \{chol(\mathbf{P}^{l-1}_k)\}^T, \tag{89}$$

$$\mathbf{X}^{l-1}_k = [\ \hat{\mathbf{x}}^{l-1}_k \quad \hat{\mathbf{x}}^{l-1}_k + \gamma\, \mathbf{S}^{l-1}_k \quad \hat{\mathbf{x}}^{l-1}_k - \gamma\, \mathbf{S}^{l-1}_k\ ], \tag{90}$$

$$\mathbf{Y}^l_k = \mathbf{h}^l(\mathbf{X}^{l-1}_k), \tag{91}$$

$$\hat{\mathbf{y}}^l_k = \sum_{i=0}^{2n} w_i^{(m)} (\mathbf{Y}^l_k)_i. \tag{92}$$

• **Measurement-update equations**

$$\mathbf{P}^l_{y_k} = \sum_{i=0}^{2n} w_i^{(c)}\ [\ (\mathbf{Y}^l_k)_i - \hat{\mathbf{y}}^l_k\ ]\ [\ (\mathbf{Y}^l_k)_i - \hat{\mathbf{y}}^l_k\ ]^T + \mathbf{R}^l_k, \tag{93}$$

$$\mathbf{P}^l_{x_k y_k} = \sum_{i=0}^{2n} w_i^{(c)}\ [\ (\mathbf{X}^{l-1}_k)_i - \hat{\mathbf{x}}^{l-1}_k\ ]\ [\ (\mathbf{Y}^l_k)_i - \hat{\mathbf{y}}^l_k\ ]^T, \tag{94}$$

$$\mathbf{K}^l_k = \mathbf{P}^l_{x_k y_k} (\mathbf{P}^l_{y_k})^{-1}, \tag{95}$$

$$\hat{\mathbf{x}}^l_k = \hat{\mathbf{x}}^{l-1}_k + \mathbf{K}^l_k \left(\ \mathbf{y}^l_k - \hat{\mathbf{y}}^l_k\ \right) \texttt{ with quaternion normalization}, \tag{96}$$

$$\mathbf{P}^l_k = \mathbf{P}^{l-1}_k - \mathbf{K}^l_k \mathbf{P}^l_{y_k} {\mathbf{K}^l_k}^T. \tag{97}$$

After finishing the last measurement update loop, set the final results be the measurement update at time $t = t_k$ as $\hat{\mathbf{x}}_k = \hat{\mathbf{x}}^r_k = \hat{\mathbf{x}}^r(k)$, $\mathbf{P}_k = \mathbf{P}^r_k$. This results become the initial condition for next time update step.

For every measurement not available at time $t = t_k$, we can skip this measurement update step. Whenever a measurement is available at any time instant $t = t_k$, that measurement can be included for this sequential measurement update processing.

Sequential Measurement Update with Sensor Latency Compensation

In Eq. (91), we need to use proper sigma points in order to calculate the nonlinear measurement model. Since GPS position and velocity measurement model use latency compensated state vector (i.e., previous

states depending on corresponding latency), measurement estimate components $\mathbf{Y}_k^l$ corresponding to GPS position and velocity are computed by using sigma points based on latency compensated states.

$$\mathbf{Y}_k^l = \mathbf{h}^l(\mathbf{X}_{k-L}^{l-1}), \tag{98}$$

where

$$\mathbf{X}_{k-L}^{l-1} = [\ \hat{\mathbf{x}}_{k-L}^- \quad \hat{\mathbf{x}}_{k-L}^- + \gamma\ \mathbf{S}_k^{l-1} \quad \hat{\mathbf{x}}_{k-L}^- - \gamma\ \mathbf{S}_k^{l-1}\ ], \tag{99}$$

and $L = \frac{Aiding\ sensor\ latency}{\Delta t}$ is time delayed steps corresponding to sensor latency.

3. Implementation

By introducing new noise definitions in Eq. (74) and (75), we have the following INS navigation process model in discrete-time state-space form:

$$\mathbf{x}_{k+1} = \mathbf{f}_d(\mathbf{x}_k, \mathbf{u}_k, k) + \mathbf{w}_k, \qquad \mathbf{w}_k \sim N(0, \mathbf{Q}_k), \tag{100}$$

$$\tag{101}$$

or

$$\begin{bmatrix} \mathbf{r}_{k+1}^n \\ \mathbf{v}_{k+1}^n \\ \mathbf{q}_{k+1} \\ \mathbf{b}_{a,k+1} \\ \mathbf{b}_{\omega,k+1} \end{bmatrix} = \begin{bmatrix} \mathbf{r}_k^n + \mathbf{v}_k^n\ \Delta t \\ \mathbf{v}_k^n + \left[\ \mathbf{C}_b^n(\mathbf{q}_k)\ (\ \bar{\mathbf{a}}_k^b - \Delta\bar{\mathbf{a}}_{imu,k}^b\ ) + \mathbf{g}^n\ \right] \Delta t \\ \left[\ \mathbf{I}_{4\times4} + \frac{1}{2}\mathbf{\Omega}(\bar{\boldsymbol{\omega}}_k^b)\ \Delta t\ \right]\ \mathbf{q}_k \\ \mathbf{b}_{a,k} \\ \mathbf{b}_{\omega,k} \end{bmatrix} + \Delta t \begin{bmatrix} \mathbf{n}_{r,k} \\ \mathbf{n}_{v,k} \\ \mathbf{n}_{q,k} \\ \mathbf{n}_{b_a,k} \\ \mathbf{n}_{b_\omega,k} \end{bmatrix}, \tag{102}$$

where
$\bar{\mathbf{a}}_k^b = \mathbf{a}_{m,k}^b - \mathbf{b}_{a,k}$ and $\bar{\boldsymbol{\omega}}_k^b = \boldsymbol{\omega}_{m,k}^b - \mathbf{b}_{\omega,k}$ are bias corrected IMU accelerometer and rate gyro measurements.

V. Simulation

Since we are targeting to develop a low-cost integrated strapdown inertial navigation system with application to Research Unmanned Aerial Vehicle (UAV),[18,19,6,16] the high-fidelity nonlinear 6-DOF simulation environment is used. The whole 6-DOF simulation code is developed with C/C++ and is equipped with neural-network-based adaptive nonlinear controller.[33] Both the EKF-based and UKF-based integrated navigation softwares are also developed in C/C++ and analyzed in the nonlinear 6-DOF simulation environment. Various meaningful nonlinear trajectories can be generated in the 6-DOF simulation. Those trajectory data are corrupted by various sources of noise based on sensor modeling. Those provide fruitful test conditions for the navigation system. In order to increase the reality of simulation model, several considerations are added. Noticing the effect of helicopter blade rotation vibration on IMU sensor measurements during flight tests,[6,16,17] the following shake vibration effects around 33 Hz are added to IMU measurements.

$$\Delta a_{shake}^b = a_{shake}\ sin(\omega_{shake}\ t), \tag{103}$$

$$\Delta\omega_{shake}^b = \omega_{shake}\ sin(\omega_{shake}\ t), \tag{104}$$

$$\tag{105}$$

where $a_{shake} = 0.1 ft/sec^2$ is accelerometer shake magnitude, $\omega_{shake} = 0.18\ rad/sec$ is rate gyro shake magnitude, and $\omega_{shake} = 2\pi * 33\ rad/sec$ is shake frequency.
The first-order lag model is used for GPS position error which is added into true GPS position instead of simple white Gaussian noise addition. GPS position error model in first-order lag model is:

$$\dot{x}(t) = -\frac{1}{T}x(t) + w(t), \tag{106}$$

where $w(t)$ is white Gaussian noise with standard deviation (0.1 ft, 0.1 ft, 0.15 ft) in each direction. This can be converted as the following discrete form:

$$x_{k+1} = \left(1 - \frac{\Delta t}{T}\right) x_k + \Delta t \; w_k, \tag{107}$$

where $\Delta t = 0.2$ sec, $T = 10$ sec.

GPS velocity error model is simple white Gaussian noise with standard deviation (0.03, 0.03, 0.05) ft/sec.

Initial accelerometer bias vector is $\mathbf{b}_a(t=0) =$ (4.5, -3.0, 0) ft/sec^2 and initial rate gyro bias is zero. These values are chosen from actual hardware characteristics.[6,16,17]

Initial position and velocity for true state and estimate state are (0, 0, 0) meter and (0, 0, 0) meter/sec, respectively. Initial attitude is ($\phi,\ \theta,\ \psi$) = (0, 0, 0) or ($q_0,\ q_1,\ q_2,\ q_3$) = (1, 0, 0, 0). Initial error covariance matrix is:

$$\begin{aligned} P = diag(\ & (5/3\ ft)^2, (5/3)^2, (7/3)^2,\ \ (3/3\ ft/sec)^2, (3/3)^2, (5/3)^2,\ \ (0.01/3)^2, (0.01/3)^2, (0.01/3)^2, (0.01/3)^2, \\ & (0.01/3\ ft/sec^2)^2, (0.01/3)^2, (0.01/3)^2,\ \ (0.01/3\ rad/sec)^2, (0.01/3)^2, (0.01/3)^2\ ). \end{aligned} \tag{108}$$

In order to assess the performance of a filter by comparing true state value and filtered estimate value, we need both true value and noise-corrupted value. The noise-corrupted value is filtered and compared with true value and then the performance of the filter is analyzed by the significance of difference between true and estimated value. In order to generate reasonable time history of IMU sensor data, full 6-DOF simulation is performed for a Pirouette trajectory motion as in Fig. 3. The resulting three-axis body accelerations (or specific forces) and three-axis angular rates generate nominal true IMU sensor outputs. This nominal sensor value is noise-corrupted with various noise sources such as bias, white Gaussian, helicopter rotor vibration effect, and so on. Simulated IMU accelerometer output and simulated IMU rate gyro output are presented in Fig. 4 and Fig. 5, respectively. GPS position data are generated with first-order lag noise model as mentioned above and are shown in Fig. 6. GPS velocity data are generated with zero-mean white Gaussian model and are shown in Fig. 7. True values are also included in these figures for comparison purpose. GPS position and velocity data are generated with latency 100 msec and 200 msec, respectively. Magnetometer sensor data are generated with zero-mean white Gaussian assumption. For the magnetometer model, the World Magnetic Model 2005 (WMM-2005) is used to generate reference magnetic field in navigation frame. This reference magnetic field is transformed to body frame and is corrupted with zero-mean Gaussian noise. The standard deviation of magnetic field noise is 0.02 in normalized magnetic field quantity. Using these artificially generated IMU, GPS, Magnetometer sensor data set, the performance of new navigation system is simulated. In order to look at the performance behavior of newly developed navigation filter based on UKF with sequential measurement, one of typical time history simulation outputs is selected and presented in Fig. 9 $\sim$ Fig. 10. The $\pm 1\sigma$ value of error covariance histories are also included in order to check error time history compared to boundary error covariance. Position error history shown in Fig. 9 and velocity error history in Fig. 10 show the fact that the state histories are well-behaved within the $\pm 1\sigma$ boundaries.

State estimate error histories using newly developed UKF navigation system are compared with the existing EKF-based navigation system in figure 11 $\sim$ Fig. 12. Figure 11(a) compares time history of RMS (root mean squared) position between EKF-based navigation system and UKF-based navigation system. RMS position error history shows that UKF-based navigation system has lower error history than that of EKF-based navigation system and thus shows better performance. The comparison in the RMS velocity error is presented in Fig. 11(b). UKF-based navigation system shows better performance in the RMS velocity history, too. Time histories of RMS accelerometer bias error and RMS rate gyro bias error are presented in Fig. 12(a) and Fig. 12(b), respectively. Time histories of RMS accelerometer bias error are similar between EKF and UKF navigation. In the comparison of RMS rate gyro bias error, error in the UKF-based system shows smaller error history. True value histories of both accelerometer and rate gyro are generated as random walk. Since we found the error performances are nearly coincided between standard UKF and sequential measurement UKF, we do not include the comparisons. Nevertheless, since the sequential measurement UKF has more advantages than standard UKF in the multi-rate sensor fusion problem, the sequential measurement UKF seems to be a better choice in our problem. The advantages of sequential measurement UKF are the easy treatment of multi-rate sensor fusion problem and sensor latency problem, easy addition of new aiding sensors in existing navigation framework while keeping the advantage of standard UKF such as no necessity of Jacobian matrices computation for nonlinear process model and measurement model.

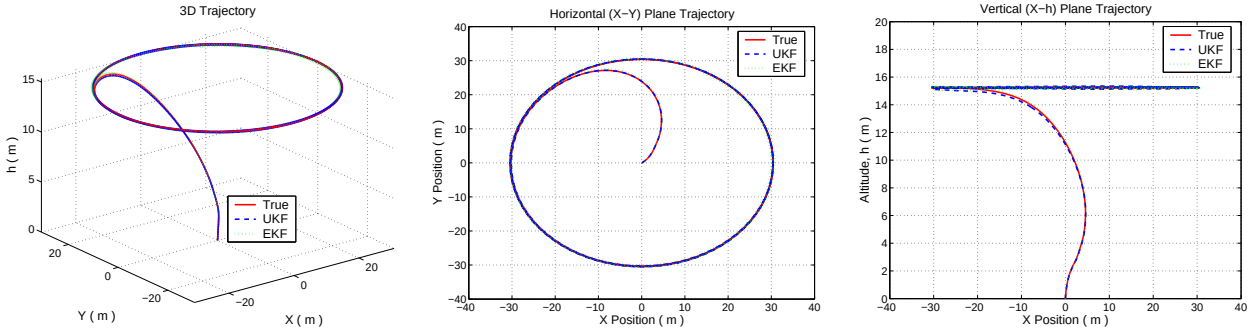

(a) 3D Trajectory (b) Position, Y vs. X (c) Position, h vs. X

Figure 3. 6-DOF Simulation Trajectory

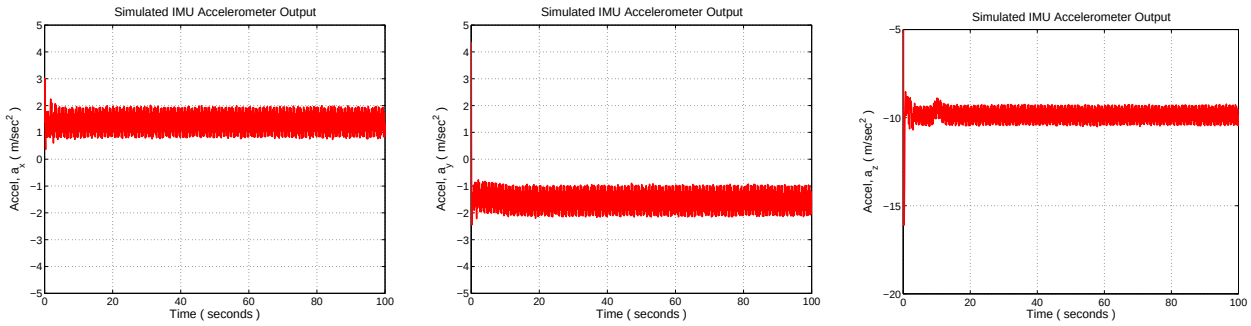

(a) a_x (b) a_y (c) a_z

Figure 4. Simulated IMU Accelerometer Triad

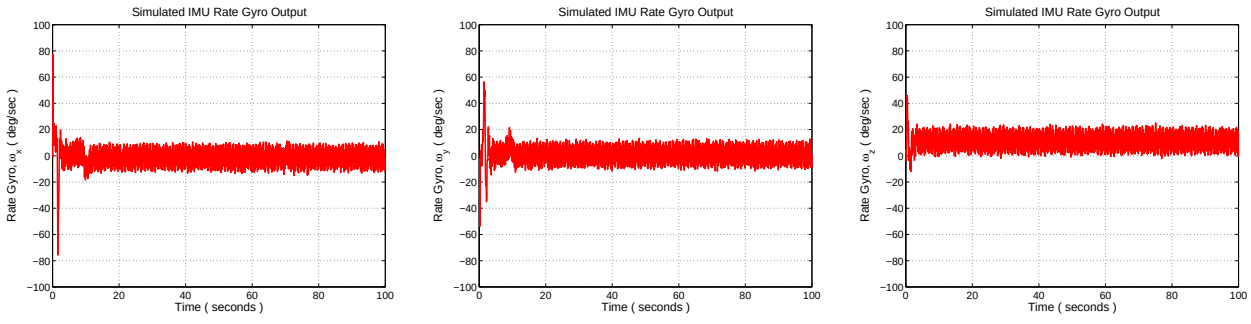

(a) ω_x (b) ω_y (c) ω_z

Figure 5. Simulated IMU Rate Gyro Triad

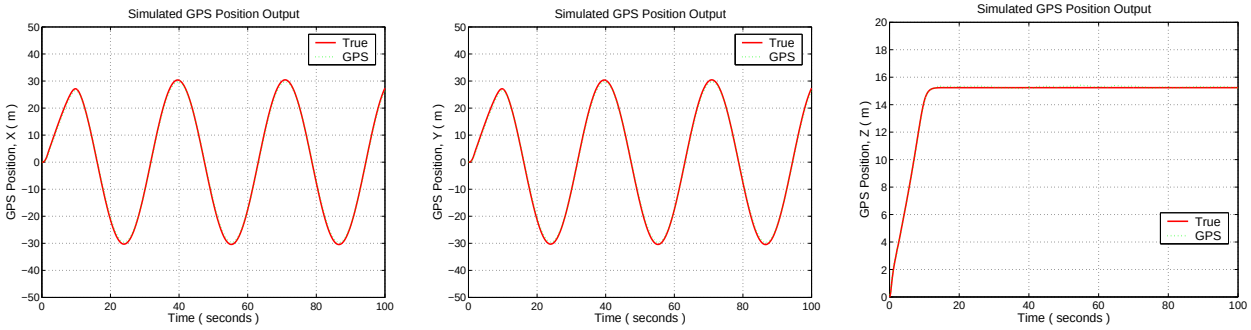

(a) Position, X (b) Position, Y (c) Altitude, h

Figure 6. Simulated GPS Position

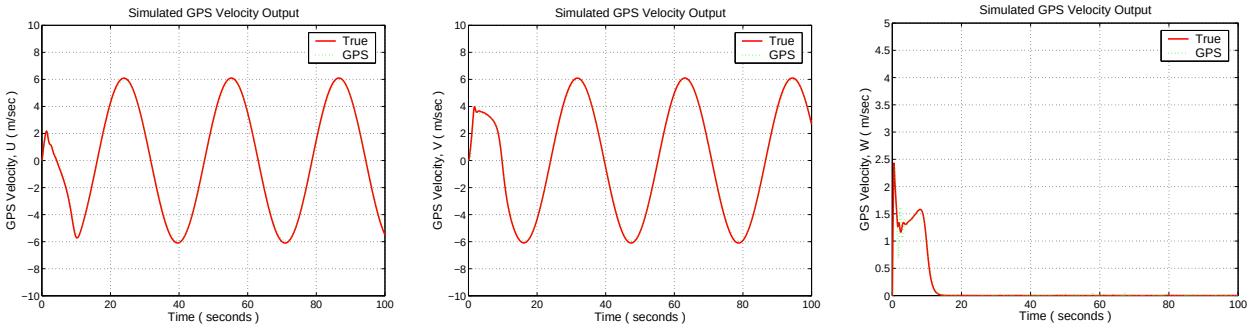

(a) Velocity, U (b) Velocity, V (c) Velocity, W

Figure 7. Simulated GPS Velocity

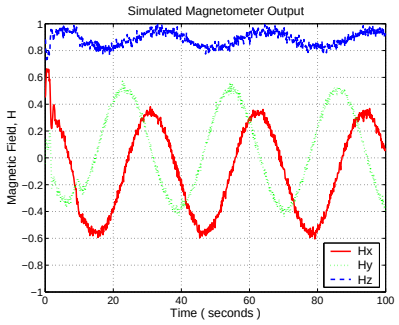

(a) Normalized H_x

Figure 8. Simulated Magnetometer Triad

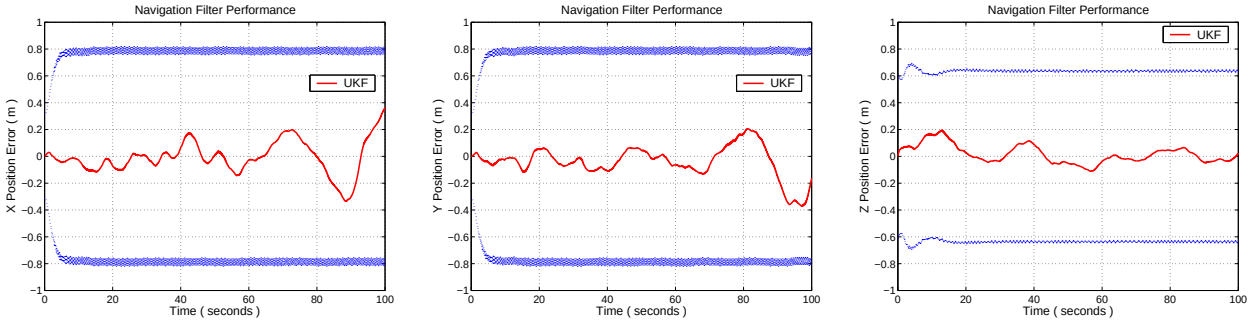

(a) X Position Error (b) Y Position Error (c) Z Position Error

Figure 9. UKF Position Error History

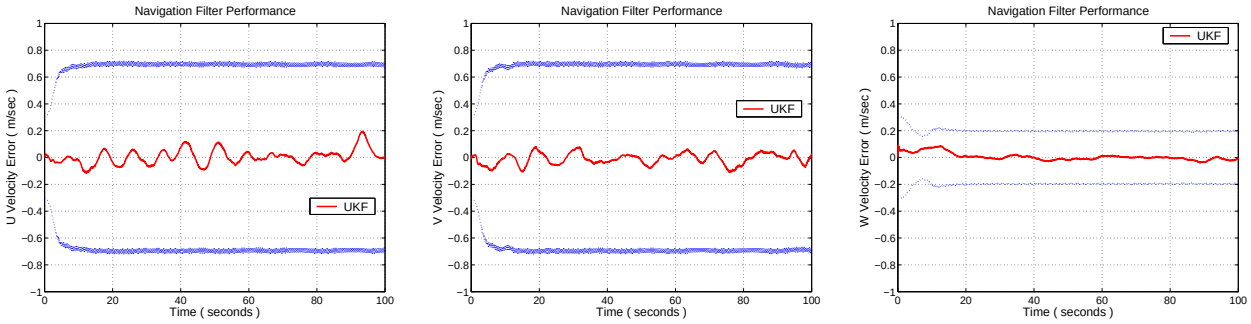

(a) U Velocity Error (b) V Velocity Error (c) W Velocity Error

Figure 10. UKF Velocity Error History

(a) RMS Position Error (b) RMS Velocity Error

Figure 11. Navigation Filter RMS Position and Velocity Error (Comparison of EKF and Sequential Measurement UKF)

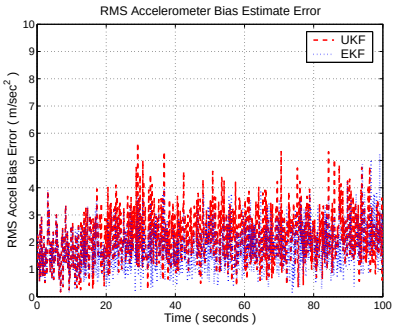

(a) RMS Accel Bias Error

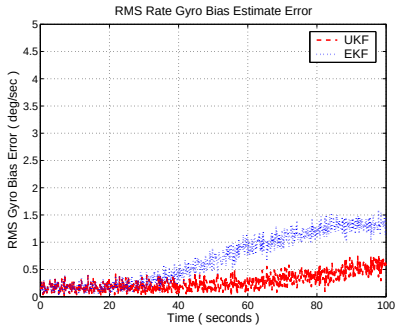

(b) RMS Rate Gyro Bias Error

Figure 12. Navigation Filter RMS Bias Error (Comparison of EKF and Sequential Measurement UKF)

VI. Conclusion

This paper discusses about the development of integrated inertial navigation system targeting to be used in the autonomous research UAV helicopter. The integrated INS is based on low-cost strapdown IMU sensors and additional aiding sensors such as DGPS, three-axis magnetometer, vision sensor, and so on. The strapdown INS navigation filter algorithm using both EKF and UKF is discussed in detail including the process model and measurement model. The resulting implementation of the EKF-based and UKF-based integrated navigation filters are compared and discussed. Both EKF-based and UKF-based integrated navigation systems have advantages and disadvantages. EKF-based navigation system needs less computational power and easy to handle multi-rate sensor fusion problem if we use sequential measurement update strategy. The necessity of messy Jocobian matrices calculation in the linearization of nonlinear process model and measurement model makes its users troublesome. On the other hand, UKF-based navigation system obviates the computation of the Jocobian matrices, but it is a bit more computationally costly. In terms of accuracy, UKF shows better performance than EKF in our low-cost integrated INS navigation system. In order to effectively deal with multi-rate sensor fusion problem in which series of different update-rate aiding sensors are fused into high-rate IMU sensor measurements, new integrated navigation algorithm based on sequential measurement UKF is developed. By using sequential measurement UKF in our integrated navigation system, we can keep the advantages such as high-order accurate nonlinear filtering, removing messy Jacobian matrices computation, and easy-handling of multi-rate, multi-sensor fusion problem with the expense of a slightly more computational cost.

References

[1]Biezad, D. J., *Integrated Navigation and Guidance Systems*, AIAA Education Series, Reston, VA, 1999.

[2]Rogers, R. M., *Applied Mathematics in Integrated Navigation Systems*, AIAA Education Series, Reston, VA, 2nd ed., 2003.

[3]Titterton, D. H. and Weston, J. L., *Strapdown Inertial Navigation Technology*, Vol. 207, AIAA, Reston, VA, 2nd ed., 2004.

[4]Kayton, M. and Fried, W. R., *Avionics Navigation Systems*, John Wiley & Sons, New York, 2nd ed., 1997.

[5]Brown, R. G. and Hwang, P. Y. C., *Introduction to Random Signals and Applied Kalman Filtering*, John Wiley & Sons, New York, 3rd ed., 1997.

[6]Dittrich, J. S. and Johnson, E. N., "Multi-sensor Navigation System for an Autonomous Helicopter," Proceedings of the 21st digital avionics systems conference.

[7]Wenger, L. and Gebre-Egziabher, D., "System Concepts and Performance Analysis of Multi-Sensor Navigation Systems for UAV Applications," Aiaa guidance, navigation, and control conference, Aug. 2003.

[8]Vasconcelos, J. F., Oliveira, P., and Silvestre, C., "Inertial Navigation System Aided by GPS and Selective Frequency Contents of Vector Measurements," Aiaa guidance, navigation, and control conference, Aug. 2004.

[9]Kingston, D. B., "Implementation Issues of Real-Time Trajectory Generation on Small UAVs," 2004.

[10]Langelaan, J. and Rock, S., "Navigation of Small UAVs Operating in Forests," Aiaa guidance, navigation, and control conference, Aug. 2004.

[11]van der Merwe, R. and Wan, E. A., "Sigma-Point Kalman Filters for Nonlinear Estimation and Sensor-Fusion - Application to Integrated Navigation," Aiaa guidance, navigation, and control conference, Aug. 2004.

[12]Maybeck, P. S., *Stochastic Models, Estimation, and Control*, Vol. 1–3, Academic Press, New York, 1979.

[13]Wan, E. A. and van der Merwe, R., "Chapter 7. The Unscented Kalman Filter," *Kalman Filtering and Neural Networks*, edited by S. Haykin, John Wiley & Sons, New York, 2001.

[14]Julier, S. J. and Uhlmann, J. K., "A New Extension of the Kalman Filter to Nonlinear Systems," Proc. of aerosense: The 11th int. symp. on aerospace/defense sensing, simulation and controls, Aug. 1997.

[15]van der Merwe, R. and Wan, E. A., "Sigma-Point Kalman Filters for Probabilistic Inference in Dynamic State-Space Models," Workshop on advances in machine learning, 2003.

[16]Dittrich, J. S., "Design and Integration of an Unmanned Aerial Vehicle Navigation System," M.s. thesis, georgia institute of technology, May 2002.

[17]Johnson, E. N. and Oh, S. M., "Development and Flight Test of Multi-sensor Navigation System for UAV Applications," Internal report, Jan. 2006.

[18]Johnson, E. N. and Schrage, D. P., "The Georgia Tech Unmanned Aerial Research Vehicle: GTMax," Aiaa guidance, navigation, and control conference, Aug. 2003.

[19]Johnson, E. N. and Schrage, D. P., "System Integration and Operation of a Research Unmanned Aerial Vehicle," *AIAA Journal of Aerospace Computing, Information, and Communication*, Vol. 1, No. 1, Jan. 2004.

[20]Gebre-Egziabher, D., Hayward, R. C., and Powell, J. D., "Design of Multi-Sensor Attitude Determination Systems," *IEEE Trans. on Aerospace and Electronic Systems*, Vol. 40, No. 2, 2004, pp. 627–649.

[21]Eck, C. and Geering, H. P., "Error Dynamics of Model Based INS/GPS Navigation for an Autonomously Flying Helicopter," Aiaa guidance, navigation, and control conference, Aug. 2000.

[22]Wendel, J., Maier, A., Metzger, J., and Trommer, G. F., "Comparison of Extended and Sigma-Point Kalman Filters for Tightly Coupled GPS/INS Integration," Aiaa guidance, navigation, and control conference, Aug. 2005.

[23]Lin, C.-F., *Modern Navigation, Guidance, and Control Processing*, Prentice Hall, Englewood Cliffs, NJ, 1991.

[24]Anderson, B. D. O. and Moore, J. B., *Optimal Filtering*, Dover Publishings, Mineola, NY, 2005.

[25]Chui, C. K. and Chen, G., *Kalman Filtering with Real-Time Applications*, Springer, New York, 3rd ed., 1999.

[26]Watanabe, Y., Johnson, E. N., and Calise, A. J., "Vision-Based Approach to Obstacle Avoidance," Aiaa guidance, navigation, and control conference, Aug. 2005.

[27]Wu, A. D., Johnson, E. N., and Proctor, A. A., "Vision-Aided Inertial Navigation," Aiaa guidance, navigation, and control conference, Aug. 2005.

[28]Stengel, R. F., *Optimal Control and Estimation*, Dover Publishings, New York, 1994.

[29]McLean, S., Maus, S., Dater, D., Macmillan, S., Lesur, V., and Thomson, A., *The US/UK World Magnetic Model for 2005-2010*, 2004, http://www.ngdc.noaa.gov/seg/WMM/data/TRWMM_2005.pdf.

[30]Julier, S. J., Uhlmann, J. K., and Durrant-Whyte, H., "A New Approach for Filtering Nonlinear Systems," Proceedings of the american control conference, Seattle, WA, 1995.

[31]Julier, S. J., Uhlmann, J. K., and Durrant-Whyte, H., "A New Method for the Nonlinear Transformation of Means and Covariances in Filters and Estimators," *IEEE Transactions on Automatic Control*, , No. 3, 2000, pp. 477–482.

[32]van der Merwe, R. and Wan, E. A., "The Square-Root Unscented Kalman Filter for State and Parameter-Estimation," Proceedings of the ieee international conference on acoustics, speech, and signal processing (icassp), May 2001.

[33]Johnson, E. N. and Kannan, S. K., "Adaptive Trajectory Control for Autonomous Helicopters," *AIAA Journal of Guidance, Control, and Dynamics*, Vol. 28, No. 3, 2005.